Journal of Materials Chemistry C

Accepted Manuscript

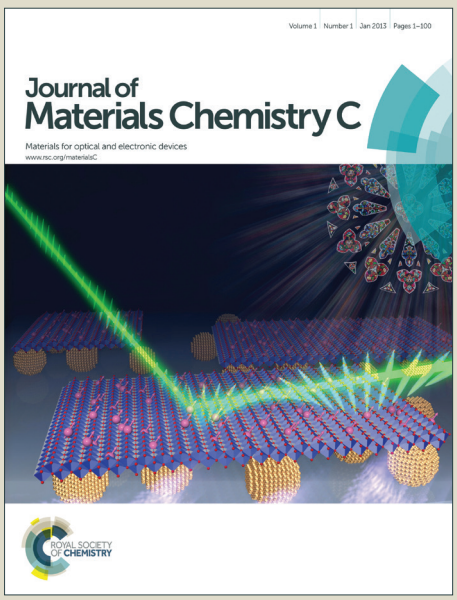

ROYAL SOCIETY OF CHEMISTRY

www.rsc.org/materialsC

Cite this: DOI: 10.1039/c0xx00000x

www.rsc.org/xxxxxx

ARTICLE TYPE

Saturable absorption and the changeover from saturable absorption to reverse saturable absorption of MoS_2 nanoflake array films†‡

Qiuyun Ouyang, Hailong Yu, Kai Zhang, Yujin Chen*

Received (in XXX, XXX) Xth XXXXXXXXX 20XX, Accepted Xth XXXXXXXXX 20XX

DOI: 10.1039/b000000x

MoS_2 nanoflake array films on different glass substrates were fabricated by an in-situ growth method. The nonlinear absorption (NLA) properties of the MoS_2 nanoflake array films were investigated by an open-aperture Z-scan technique. The MoS_2 nanoflake array films exhibited different NLA properties dependent on the input energy. In the case of the lower input energy, the film exhibited saturable absorption (SA); however, if the input energy was increased, a changeover from SA to reverse saturable absorption (RSA) was observed. The interesting NLA properties of the film could be attributed to the competition between the ground-state absorption and the excited-state absorption in terms of energy-level model of MoS_2.

1 Introduction

Layered materials represent a diverse and largely untapped source of two-dimensional (2D) systems with exotic optical and electronic properties that are important for energy storage, optical limiting, laser, sensing, and catalysis applications.[1, 2] Recently, transition metal dichalcogenides (TMDs) have been of renewed interest materials for a variety of applications in optical and electronic devices.[3–19] Among TMDs, MoS_2 is an n-type semiconductor with an indirect band gap of ~1.2 eV in the bulk form.[9] It has large in-plane carrier mobility (around 200–500 $cm^2V^{-1}s^{-1}$)[10] and good photoelectrochemical stability.[11] Moreover, the band gap of MoS_2 increases with decreasing crystal thickness due to quantum confinement. Theoretical calculations predict that the band gap of MoS_2 with a monolayer is increased to about 1.9 eV, and in the case MoS_2 will possess characteristics of direct band gap semiconductors.[12] The indirect-to-direct gap transition of MoS_2 could result in giant enhancement (~10^4) in photoluminescence (PL) quantum yield.[4] In addition, both PL and absorption of monolayer MoS_2 can be controlled by gate voltage.[13] Therefore, MoS_2 has attracted great interest due to its distinctive electronic, optical, catalytic, and lubricating properties with potential applications such as solar cells,[5] photocatylysis,[6] and field-effect transistors.[7, 8]

The steady-state and transient optical absorption spectra of few-layer MoS_2 have been recently reported.[20–22] However, to the best of our knowledge, the research regarding the nonlinear optical (NLO) properties of MoS_2 nanoflake array films have not been studied. Herein, the MoS_2 nanoflake array films on different glass substrate were fabricated by an in-situ growth method. Their nonlinear absorption (NLA) properties were investigated by an open-aperture Z-scan technique.[23] The MoS_2 nanoflake array films exhibited different NLA properties dependent on the input energy, and the related mechanism was discussed.[24]

2 Experimental sections

2.1 Fabrication of MoS_2 nanoflake array films

The MoS_2 nanoflake array films were fabricated using an in-situ growth method.[2, 25] In a typical process, MoO_3 (30 mg), thiacetamide (35 mg), and urea (0.3 g) were dispersed in 40 mL of ethanol under vigorously stirring for 1 h. Then a glass trestle was put into a Teflon-lined stainless autoclave with a capacity of 50 mL, and the well-cleaned F-doped SnO_2 (FTO) glass substrate was placed on the glass trestle (the conductive side of the FTO glass substrate is against the bottom of the Teflon-lined stainless autoclave). After that the mixture was then transferred into the Teflon-lined stainless steel autoclave for hydrothermal treatment at 200°C for 24 h. As the autoclave was cooled to room temperature naturally, the sample was washed with distilled water and absolute ethanol, the side of insulation should be wipe by lens paper and dried in a vacuum oven at 40°C for 12 h. For simplicity, the sample was denoted as FTO/MoS_2 film. The quartz/MoS_2 film as compared sample was also fabricated according to the above process.

2.2 Characterizations of FTO/MoS_2 and quartz/MoS_2 films

The morphologies of FTO/MoS_2 and quartz/MoS_2 films were characterized by scanning electron microscopy (SEM, JEOL-JSM-6700F), an FEI Tecnai-F20 transmission electron microscope (TEM) and atomic force microscopy (AFM). Raman and UV-visible (UV-vis) absorption spectra of FTO/MoS_2 and quartz/MoS_2 films were measured by Renishaw Raman spectrometer and Shimadzu UV-2450 spectrometer, respectively.

2.3 NLA measurements of FTO/MoS_2 and quartz/MoS_2 films

The NLA properties of FTO/MoS_2 and quartz/MoS_2 films were investigated using an open-aperture (OA) Z-scan technique.[23] The laser used in the measurement was an Nd:YAG laser system, which produced 6 ns laser pulses at 532 nm with a repetition rate of 1 Hz. The spatial distribution of the laser pulses exhibited a nearly Gaussian profile. The input and output energies of the laser pulses were measured by energy meters (Laser energy meter

WIR-68254). The investigated samples were mounted on a mobile platform controlled by a computer that moved the sample along the *z*-axis through the focal plane of 150 mm focal length lens. The beam waist radius ($1/e^2$ radius) in the focal plane was 47 μm and the input energy was in the range of 10–35 μJ (the input peak light intensity at focus was in the range of 48.3–169 $MWcm^{-2}$), which was lower than the damage threshold of FTO/MoS_2 and quartz/MoS_2 films (~83 μJ, corresponding to the peak light intensity about 400 $MWcm^{-2}$).

3 Results and discussions

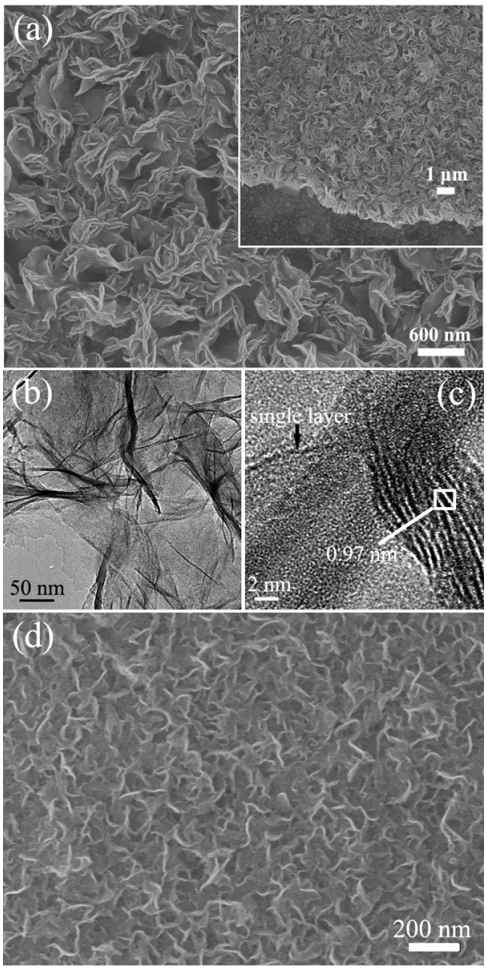

Fig. 1 (a) SEM image of the FTO/MoS_2 film measured at the middle part. The inset is SEM image of the FTO/MoS_2 film measured at the edge part; (b) TEM and (c) HRTEM images of MoS_2 nanoflakes on the FTO glass substrate; (d) SEM image of the quartz/MoS_2 film.

Fig. 1(a) shows a typical SEM image of the FTO/MoS_2 film. It can be clearly found that the MoS_2 nanoflakes with lengths of 600–1000 nm are uniformly and densely grown on the surface of the FTO glass substrate. The inset of Fig. 1(a) shows that the thickness of MoS_2 nanoflake array film on the FTO glass substrate is smaller than 1 μm. The atomic force microscopy (AFM) measurement showed that the thickness of MoS_2 nanoflake array film on the FTO glass substrate is about 730 nm (Fig. S1). TEM image (Fig. 1(b)) shows that the thickness of an individual MoS_2 nanoflake is less than 10 nm. High resolution TEM (HRTEM) image (Fig.1(c)) shows that the interlayer distance of (002) crystal plane of MoS_2 nanoflakes (marked by a white frame) is about 0.97 nm. Furthermore, single layered MoS_2 nanoflakes are also observed in the HRTEM image. In contrast, the bulk MoS_2 materials have an interlayer distance of the (002) plane of 0.616 nm. The results reveal that the spacing of the (002) crystal plane of MoS_2 nanoflakes on the FTO glass substrate is significantly expanded, similar to our previous results.[26] Fig. 1(d) shows the SEM image of the quartz/MoS_2 film. The lengths of the MoS_2 nanoflakes on the quartz glass substrate are about 100–200 nm, which are smaller than those of the MoS_2 nanoflakes on the FTO glass substrate.

Fig. 2(a) shows the Raman spectra of FTO/MoS_2 film and FTO glass substrate. The peaks at 379 cm^{-1} and 407 cm^{-1} in the spectrum FTO/MoS_2 film, ascribed to E^1_{2g} (in-layer displacement of molybdemum and sulfur atoms) and A1g (out-of-layer symmetric displacement of sulfur atoms along *c* axis) modes, respectively, are typically characteristic peaks of hexagonal MoS_2.[27, 28] However, there are no peaks at 379 cm^{-1} and 407 cm^{-1} in the Raman spectrum of the FTO glass substrate. This reveals that MoS_2 is successfully grown on the FTO glass substrate. Fig. 2(b) shows UV-vis absorption spectra of FTO/MoS_2 film, FTO glass substrate, quartz/MoS_2 film and quartz glass substrate. It is obvious that the FTO/MoS_2 film exhibits the strongest linear absorption. As for the quartz/MoS_2 film, there is a broad absorption peak in the wavelength range of 350–400 nm. The absorbance of the quartz glass substrate is almost zero in the wavelength range of 300–800 nm.

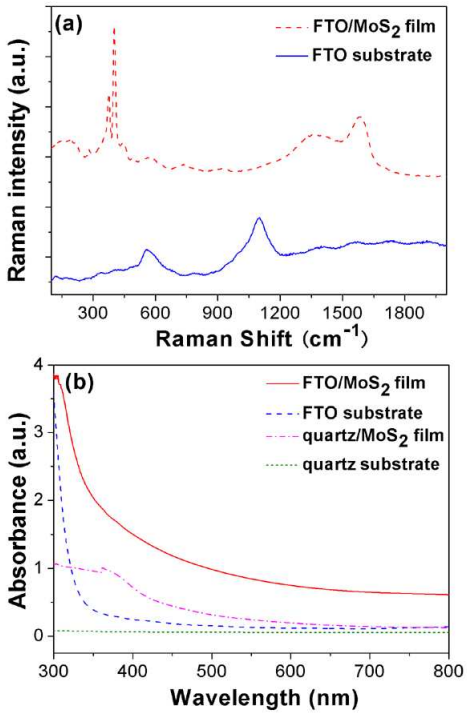

Fig. 2 (a) Raman spectra and (b) UV-vis absorption spectra of FTO/MoS_2 film, FTO glass substrate, quartz/MoS_2 film and quartz glass substrate.

Photographs of FTO/MoS_2 film, FTO glass substrate, quartz/MoS_2 film and quartz glass substrate are shown in Fig. 3(a), (b), (c) and (d), respectively. Both colours of FTO/MoS_2 film and quartz/MoS_2 film dark-brown, and colours of FTO glass substrate and quartz glass substrate are colourless. The "HRBEU"

letters underneath the glass are visualized by the naked eye, suggesting that both FTO/MoS_2 film and quartz/MoS_2 film are also transparent to visible light.

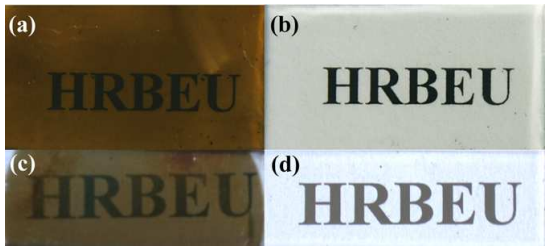

Fig. 3 Photographs of (a) FTO/MoS_2 film; (b) FTO glass substrate; (c) quartz/MoS_2 film and (d) quartz glass substrate.

In order to explore the input energy dependence of NLA of FTO/MoS_2 and quartz/MoS_2 films, the samples are scanned at the same position with increasing and decreasing the input energy. As comparison, the FTO and quartz glass substrates are also measured with the same method. As shown in Fig. 4(a)–(h), at the beginning, there are no transmission variations for all samples at low input energy of 10 μJ. From Fig. 4(a) and (b), it can be seen that when the input energy is increased to be 18 μJ, the FTO/MoS_2 film exhibits an increase of transmittance at positions close to the focus, a typical saturable absorption (SA) effect. When the input energy is increased to be 20 μJ, the FTO/MoS_2 film begins to exhibit a change from SA to reverse saturable absorption (RSA). When the input energy is continued increasing to be 22 and 28 μJ, the FTO/MoS_2 film still exhibits a change from SA to RSA, and the higher input energy corresponding to the deeper valley at focus. As the input energy is increased to be 35 μJ, the FTO/MoS_2 film completely changes from SA to RSA. Then the input energy is decreased to be 19 μJ, the FTO/MoS_2 film shows a trend of change from RSA back to SA. When the input energy is increased to be 17 μJ, the FTO/MoS_2 film completely changes from RSA back to SA. Finally, the input energy is decreased to be the lowest input energy of 10 μJ, there is no transmission variation in the OA Z-scan curve of the FTO/MoS_2 film. Concisely, the OA Z-scan curves reveal a change from SA to RSA while increasing the input energy, and the change from RSA back to SA while decreasing the input energy indicates the sample is not damaged.[29]

Fig. 4(c) and (d) show the OA Z-scan curves of the FTO glass substrate when increasing and decreasing the input energy. When the input energy is lower (18 and 20 μJ), the FTO glass substrate exhibits a SA effect. When the input energy is increased to be 22 μJ, the FTO glass substrate exhibits a change from SA to RSA. When the input energy is increased to be 28 and 35 μJ, the FTO glass substrate exhibits a RSA effect. While decreasing the input energy, the FTO glass substrate exhibits a change from RSA back to SA, which indicates that the FTO glass substrate is not damaged. However, at the same input energy, the peaks or valleys of the OA Z-scan curves of the FTO/MoS_2 film are higher or deeper than those of the FTO glass substrate, which indicates that the FTO/MoS_2 film exhibits enhanced NLA properties.

Fig. 4(e) and (f) show the OA Z-scan curves of the quartz/MoS_2 film. The quartz/MoS_2 film exhibits similar NLA properties to the FTO/MoS_2 film. When the input energies are 20 and 24 μJ, the valleys in the OA Z-scan curves of the quartz/MoS_2 film are obviously deeper than those of the FTO/MoS_2 film. While the input energies are 18 and 19 μJ, the peaks in the OA Z-scan curves of the quartz/MoS_2 film are lower than those of the FTO/MoS_2 film.

There is no obvious NLA observed in the quartz glass substrate in the input energy range of 10–35 μJ. The Z-scan curve of the quartz glass substrate at the input energy of 35 μJ is shown in Fig. 4(g).

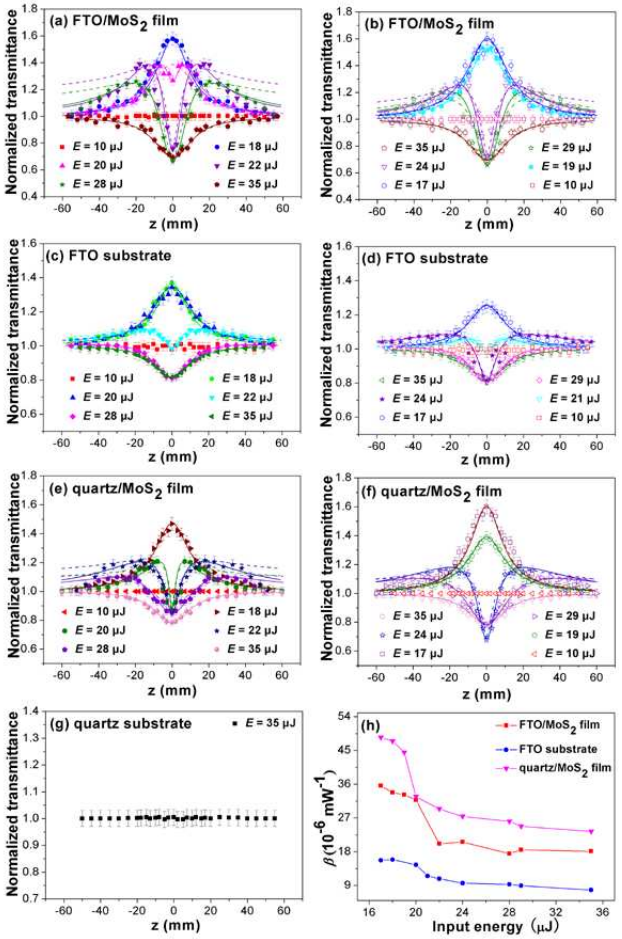

Fig. 4 The OA Z-scan curves of the FTO/MoS_2 film (a) while increasing the input energy and (b) decreasing the input energy; the OA Z-scan curves of the FTO glass substrate (c) while increasing the input energy and (d) decreasing the input energy; the OA Z-scan curves of the quartz/MoS_2 film (e) while increasing the input energy and (f) decreasing the input energy; (g) the OA Z-scan curve of the quartz glass substrate; and (h) the comparison of β_2 values via the input energy among FTO/MoS_2 film, FTO glass substrate, and quartz/MoS_2 film. All solid lines and dashed lines in Fig. 4(a)–(f) are fitting curves using Eq. (1)–(3) and Eq. (4)–(5), respectively.

In order to obtain the nonlinear absorption coefficient, the experimental data are analyzed by a model related to both SA and RSA.[30–32] The total absorption coefficient $\alpha(I)$ can be expressed as:[30–32]

$$\alpha(I) = \frac{\alpha_0}{1 + I / I_s} + \beta_1 I, \quad (1)$$

where α_0 is the linear absorption coefficient which can be obtained from UV-vis spectra. I is the laser light intensity, and I_s is the saturation light intensity. β_1 is nonlinear absorption

coefficient. Therefore the modified normalized transmittance using Eq. (1) can be written as:[31]

$$T(z) = \frac{Q(z)}{\sqrt{\pi}q(z)}\int_{-\infty}^{+\infty}\ln\left[1+q(z)\exp(-\tau^2)\right]d\tau, \quad (2)$$

where

$$\begin{aligned} Q(z) &= \exp\left[\alpha_0 LI/(I+I_s)\right] \\ q(z) &= \beta_1 I_0 L_{eff}/(1+z^2/z_0^2) \end{aligned} \quad (3)$$

I_0 is the peak light intensity at focus; $L_{eff} = [1-\exp(-\alpha_0 L)]/\alpha_0$ is the effective thickness of the sample; L is the thickness of the sample. $z_0 = \pi w_0^2/\lambda$ is the Rayleigh range, where w_0 is the beam waist radius; and λ is the wavelength of the incident light.

The thicknesses of MoS_2 nanoflake array films on FTO and quartz glass substrates are 730 and 224 nm (Fig. S1 and S2), respectively. Because the surface of the quartz glass substrate is smoother than that of the FTO glass substrate, therefore the thickness of the MoS_2 nanoflake array film on the quartz glass substrate is thinner. The contribution of FTO nanofilm with the thickness of 400 nm to the NLA is considered (Fig. S3), therefore the total thickness of the FTO/MoS_2 film should be 1130 nm. Because there is no obvious NLA observed in the quartz glass substrate, therefore the thickness of the quartz/MoS_2 film is 224 nm. The values of linear transmittance T_0 and α_0 at 532 nm of FTO/MoS_2 film, FTO glass substrate and quartz/MoS_2 film can be obtained from UV-vis spectra. The solid lines in Figs. 4(a)–(f) are the fitting curves using Eq. (1)–(3).

The values of linear transmittance T_0 and α_0 of the FTO/MoS_2 film obtained from UV-vis spectra are 41.1% and 0.79 μm^{-1}, respectively. According to Eq. (1)–(3), the calculated values of β_1 and I_s of the FTO/MoS_2 film can be obtained, listed in Table 1. From Table 1, it can be seen that the β_1 value of the FTO/MoS_2 film increases firstly, and then decreases with the increasing of the input energy. At the input energy of 22 μJ, the β_1 value of the FTO/MoS_2 film is the largest and the I_s value is the lowest.

Table 1 The values of β_1 and I_s of the FTO/MoS_2 film with different input energies obtained according to Eq. (1)–(3), and the values of β_2 and τ_1 obtained according to Eq. (4) and (5).

E (μJ)	β_1 (10^{-6}mW^{-1})	I_s (MWcm^{-2})	β_2 (10^{-6}mW^{-1})	τ_1 (ps)
17	–0.98	302	35.6	717.89
18	–0.86	302	33.8	717.88
19	–0.72	302	33.2	717.88
20	3.32	20.4	31.8	717.92
22	13.2	5.05	19.7	718.13
24	13.0	8.25	21.9	718.11
28	12.9	8.45	17.5	718.13
29	12.5	10.5	18.5	718.12
35	6.58	64.4	18.1	718.07

The values of linear transmittance T_0 and α_0 of the FTO glass substrate obtained from UV-vis spectra are 87.4% and 0.31 μm^{-1}, respectively. The calculated values of β_1 and I_s of the FTO glass substrate obtained according to Eq. (1)–(3) are listed in Table 2. The β_1 value of the FTO glass substrate also increases firstly, and then decreases with the increasing of the input energy. At the input energy of 24 μJ, the β_1 value of the FTO glass substrate is the largest and the I_s value is the lowest. On the whole, the values of β_1 of the FTO glass substrate are smaller than those of the FTO/MoS_2 film at the same input energy.

Table 2 The values of β_1 and I_s of the FTO glass substrate with different input energies obtained according to Eq. (1)–(3), and the values of β_2 and τ_1 obtained according to Eq. (4) and (5).

E (μJ)	β_1 (10^{-6}mW^{-1})	I_s (MWcm^{-2})	β_2 (10^{-6}mW^{-1})	τ_1 (ps)
17	–1.31	106	15.7	717.96
18	–1.69	106	15.9	717.86
20	–1.45	106	14.5	717.86
21	1.23	10.9	11.5	718.01
22	1.25	2.76	10.8	718.01
24	3.18	1.66	9.63	718.05
28	2.53	26.6	9.30	718.03
29	2.49	26.6	8.94	718.03
35	1.77	95.6	7.79	718.01

The values of linear transmittance T_0 and α_0 of the quartz/MoS_2 film are 78.6% and 1.18 μm^{-1}, respectively. The calculated values of β_1 and I_s of the quartz/MoS_2 film obtained according to Eq. (1)–(3) are listed in Table 3. The β_1 value of the quartz/MoS_2 film also increases firstly, and then decreases with the increasing of the input energy. At the input energy of 24 μJ, the β_1 value is the largest and the I_s value is the lowest. At the input energies of 17 and 18 μJ, the I_s values of both quartz/MoS_2 film and FTO glass substrate are 106 MWcm^{-2}, which is half of that of the FTO/MoS_2 film.

Table 3 The values of β_1 and I_s of the quartz/MoS_2 film with different input energies obtained according to Eq. (1)–(3), and the values of β_2 and τ_1 obtained according to Eq. (4) and (5).

E (μJ)	β_1 (10^{-6}mW^{-1})	I_s (MWcm^{-2})	β_2 (10^{-6}mW^{-1})	τ_1 (ps)
17	–4.35	106	48.5	717.79
18	–3.36	106	47.5	717.80
19	–2.64	106	44.5	717.85
20	9.18	1.13	32.7	718.05
22	8.95	1.09	29.4	718.05
24	15.8	1.09	27.4	718.08
28	6.75	9.85	26.1	718.03
29	8.58	7.05	24.8	718.04
35	6.35	89.5	23.4	718.01

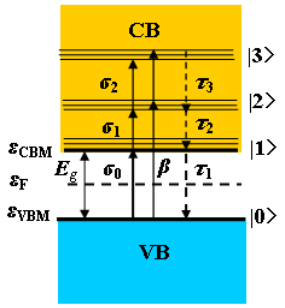

Fig. 5 Energy-level diagram of MoS_2 nanoflake array film. E_g, the band gap; σ_0, ground-state absorption cross section, σ_1 and σ_2, excited state absorption cross sections from states |1> and |2>, respectively; β_2, 2PA coefficient; $\tau_{1,2,3}$, excited states lifetimes of |1>, |2>, |3>, respectively.

In order to investigate the NLA dynamic process of FTO/MoS_2 and quartz/MoS_2 films, the energy-level diagram of MoS_2 nanoflake array film is given as shown in Fig. 5.[32–34] In general, NLA properties of semiconductors in the visible range basically originate from two mechanisms, namely interband and intraband

transitions. Because the band gap of MoS_2 (E_g = 1.2–1.9 eV) is smaller than that of photon energy (2.33 eV), both interband and intraband transitions of MoS_2 can contribute to NLA of FTO/MoS_2 and quartz/MoS_2 films. For the nanosecond laser, the pulse width is much longer than the intraband relaxation time (τ_2 and τ_3 are on the order of femtosecond).[34, 35] Hence the equations governing the NLA process in the nanosecond regime can be expressed as:[34, 36–38]

$$\frac{\partial I}{\partial z'} = -\alpha I = -(\alpha_0 + N_{ex}\sigma_{eff} + \beta_2 I)I \,, \quad (4)$$

$$\frac{\partial N_{ex}}{dt} = \frac{\alpha_0 I}{h\nu} - \frac{N_{ex}}{\tau_1} + \frac{\beta_2 I^2}{2h\nu} \quad (5)$$

where N_{ex} is the carrier density of the lowest level of conduction band, i.e. the state |1> (the ground-state carrier density is denoted as N_0), and $h\nu$ is photon energy (2.33 eV); σ_{eff} is the effective free carrier absorption (FCA) cross section, which is related to σ_1 and σ_2; α_0 ($\alpha_0 = N_0\sigma_0$) and β_2 are the linear absorption and two-photon absorption (2PA) coefficients arising from the transitions of |0>→|1> and |0>→|2>, respectively; τ_1 is the interband relaxation time; z' is the coordinate inside the nonlinear sample which changes from zero to L, and L is the thickness of sample. I is the laser light intensity.

According to Eq. (4) and (5), we used the four-order Runge-Kutta method to fit the experimental data of FTO/MoS_2 film, FTO glass substrate and quartz/MoS_2 film. The dashed lines in Fig. 4(a)–(f) show the fitting the results. During the fitting processes, the σ_{eff} value is fixed as 3.04×10^{-21} m^2 for all samples.[36] The N_0 values of FTO/MoS_2 film, FTO glass substrate and quartz/MoS_2 film are 2.525×10^{28}, 6.329×10^{28} and 1.130×10^{29} m^{-3}, respectively. The values of β_2 and τ_1 of FTO/MoS_2 film, FTO glass substrate and quartz/MoS_2 film with different input energies obtained according to Eq. (4) and (5) are listed in Table (1), (2) and (3), respectively.

Because the contributions of the higher states |2> and |3> to the NLA are neglected, the dashed lines are not as good as the solid lines to fit the experimental data. The comparison of β_2 values via the input energy among FTO/MoS_2 film, FTO glass substrate, and quartz/MoS_2 film is shown in Fig. 4(h). For three samples, the β_2 values decreases with the increasing the input energy, which is due to the saturation of RSA.[36] In addition, the β_2 values of the quartz/MoS_2 film are largest at the same input energy among three samples, which is related to the thinner thickness of the quartz/MoS_2 film.

From Table 1–3, it can be seen that when the input energy is lower, the τ_1 values are smaller, i.e. the excited carriers can quickly return back to the ground-state |0>, the ground-state absorption plays dominate role, therefore the samples exhibit SA. While the input energy is higher, the τ_1 values become larger, i.e. the excited carriers slowly return back to the ground-state |0>, the excited-state absorption plays dominate role, leading to the change from SA to RSA or complete RSA.

The calculated τ_1 values of FTO/MoS_2 film, FTO glass substrate, and quartz/MoS_2 film are in the same order of the interband transition time of semiconductor materials (0.8 ns).[34] We further compared the values of α_0, β_2 and I_s of FTO/MoS_2 and quartz/MoS_2 films with those of the MoS_2 dispersions excited by the femtosecond laser.[35] The α_0 values of FTO/MoS_2 and quartz/MoS_2 films are 0.79 and 1.18 μm^{-1}, respectively, which are about 3 orders of magnitude larger than those of the MoS_2 dispersions. The β_2 values of both FTO/MoS_2 and quartz/MoS_2 films are in the order of $10^{-5}mW^{-1}$, which are about 9 orders of magnitude larger than those of the MoS_2 dispersions. The I_s values of FTO/MoS_2 and quartz/MoS_2 films are in the range of several to several hundred $MWcm^{-2}$, which are much lower than those of the MoS_2 dispersions (several hundred $GWcm^{-2}$), therefore, the SA effect and the changeover from SA to RSA can be easier realized in FTO/MoS_2 and quartz/MoS_2 films. In addition, the larger linear and nonlinear absorption coefficients and smaller heat conductivity (0.1 $Wm^{-1}K^{-1}$), which can cause the absorbed optical heat not easy to loose and local heat up, correspondingly affects on the NLO properties both of FTO/MoS_2 and quartz/MoS_2 films.[39]

4 Conclusions

In summary, the MoS_2 nanoflake array films on FTO and quartz glass substrates were fabricated by an in-situ growth method. The NLA properties of MoS_2 nanoflake array films were investigated by using nanosecond Z-scan technique. The experimental data were simulated by using the modified Z-scan theory and simplified rate equations. The MoS_2 nanoflake array films could exhibit SA and the changeover from SA to RSA by adjusting the input energy. The NLA dynamic process of the MoS_2 nanoflake array films have been analyzed by applying the four energy-level model. Due to good NLA properties and fast response time, the MoS_2 nanoflake array films are very promising for optical devices such as ultrafast lasers and ultrafast optical switches.

Acknowledgements

This work was supported by the National Natural Science Fund of China (Grant Nos. 61205113, 51072038 and 51272050), Program for New Century Excellent Talents in University (NECT-10-0049), and also the 111 project (B13015) of Ministry Education of China to the Harbin Engineering University.

Notes and references

Address: Key Laboratory of In-Fiber Integrated Optics of Ministry of Education, College of Science, Harbin Engineering University, Harbin 150001, China.
E-mail: chenyujin@hrbeu.edu.cn

† Electronic Supplementary Information (ESI) available: [details of any supplementary information available should be included here]. See DOI: 10.1039/b000000x/

‡ Q. Y. Ouyang and H. L. Yu contributed equally to this work.

1 J. N. Coleman, M. Lotya, A. ONeill, S. D. Bergin, P. J. King, U. Khan, K. Young, A. Gaucher, S. De, R. J. Smith, I. V. Shvets, S. K. Arora, G. Stanton, H. Y. Kim, K. Lee, G. T. Kim, G. S. Duesberg, T. Hallam, J. J. Boland, J. J. Wang, J. F. Donegan, J. C. Grunlan, G. Moriarty, A. Shmeliov, R. J. Nicholls, J. M. Perkins, E. M. Grieveson, K. Theuwissen, D. W. McComb, P. D. Nellist and V. Nicolosi, *Science* 2011, **331**, 568–571.

2 Q. Y. Ouyang, H. L. Yu, Z. Y. Lei, L. H. Qi and Y. J. Chen, *Opt. Mater.* **35**, 2013, 2352–2356.

3 A. Splendiani, L. Sun, Y. Zhang, T. Li, J. Kim, C. Y. Chim, G. Galli and F. Wang, *Nano Lett.* 2010, **10**, 1271–1275.

4 K. F. Mak, C. Lee, J. Hone, J. Shan and T. F. Heinz, *Phys. Rev. Lett.* 2010, **105**, 136805.

5 A. Dashora, U. Ahuja and K. Venugopalan, *Comp. Mater. Sci.* 2013, **69**, 216–221.
6 X. Zong, H. J. Yan, G. P. Wu, G. J. Ma, F.Y. Wen, L. Wang and C. Li, *J. Am. Chem. Soc.* 2008, **130**, 7176–7177.
7 B. Radisavljevic, A. Radenovic, J. Brivio, V. Giacometti and A. Kis, *Nat. Nanotechnol.* 2011, **6**, 147–150.
8 S. Ghatak, A. N. Pal and A. Ghosh, *ACS Nano* 2011, **5**, 7707–7712.
9 C. Lee, H. Yan, L. E. Brus, T. F. Heinz, J. Hone and S. Ryu, *ACS Nano* 2010, **4**, 2695–2700.
10 G. Eda, H. Yamaguchi, D. Voiry, T. Fujita, M. Chen and M. Chhowalla, *Nano Lett.* 2011, **11**, 5111–5116.
11 T. Moehl, M. Kunst, F. Wunsch and H. Tributsch, J. Electroanal. Chem. 2007, **609**, 31–41.
12 T. S. Li and G. L. Galli, *J. Phys. Chem. C* 2007, **111**, 16192–16190.
13 A. K. M. Newaz, D. Prasai, J. I. Ziegler, D. Caudel, S. Robinson, R. F. Haglund Jr. and K. I. Bolotin, *Solid State Commun.* 2013, **155**, 49–52.
14 C. Ataca, M. Topsakal, E. Aktürk and S. Ciraci, *J. Phys. Chem. C* 2011, **115**, 16354–16361.
15 A. Kuc, N. Zibouche and T. Heine, *Phys. Rev. B* 2011, **83**, 245213.
16 S. Tongay, J. Zhou, C. Ataca, K. Lo, T. S. Matthews, J. B. Li, J. C. Grossman and J. Q. Wu, *Nano Lett.* 2012, **12**, 5576–5580.
17 Z. Li and J. P. Carbotte, *Phys. Rev. B* 2012, **86**, 205425.
18 A. Splendiani, L. Sun, Y. B. Zhang, T. S. Li, J. Kim, C. Y. Chim, G. Galli and F. Wang, Nano Lett. 2010, **10**, 1271–1275.
19 T. Korn, S. Heydrich, M. Hirmer, J. Schmutzler and C. Schüller, *Appl.Phys.Lett.* 2011, **99**, 102109.
20 E. Fortin and F. Raga, *Phys. Rev. B* 1975, **11**, 905–912.
21 R. Wang, B. Ruzicka, N. Kumar and M. Bellus, *Phys. Rev.B* 2012, **86**, 045406.
22 H. Y. Shi, R. S. Yan, S. Bertolazzi, J. Brivio, B. Gao, A. Kis, D. Jena, H. G. Xing and L. B. Huang, *ACS Nano* 2013, **7**, 1072–1080.
23 M. Sheik-Bahae, A. A. Said, T. -H. Wei, D. J. Hagan and E. W. V. Stryland, *IEEE J. Quantum. Electron.* 1990, **26**, 760–769.
24 S. Kumar, M. Anija, N. Kamaraju, K. S. Vasu, K. S. Subrahmanyam, A. K. Sood and C. N. R. Rao, *Appl. Phys. Lett.* 2009, **95**, 191911.
25 H. W. Wang, P. Skeldon and G. E. Thompson, *Surf. Coat. Technol.* 1997, **91**, 200.
26 H. L. Yu, C. L. Zhu, K. Zhang, Y. J. Chen, C. Y. Li, P. Gao, P. P. Yang and Q. Y. Ouyang, *J. Mater. Chem. A* 2014, **2**, 4551–4557.
27 J. Xiao, X. J. Wang, X. Q. Yang , S. D. Xun, G. Liu, P. K. Koech, J. Liu and J. P. Lemmon, *Adv. Funct. Mater.* 2011, **21**, 2840–2846.
28 H. L. Yu, C. Ma, B. H. Ge, Y. J. Chen, Z. Xu, C. L. Zhu, C. Y. Li, Q. Y. Ouyang, P. Gao, J. Q. Li, C. W. Sun, L. H. Qi, Y. M. Wang and F. H. Li, *Chem. Eur. J.* 2013, **19**, 5818–5823.
29 F. Li, P. X. Lu, H. Long, G. Yang, Y. H. Li and Q. G. Zheng, *Opt. Express* 2008, **16**, 14571–14581.
30 Y. C. Gao, X. R. Zhang,Y. L. Li, H. F. Liu, Y. X. Wang, Q. Chang, W. Y. Jiao and Y. L. Song, *Opt. Commun.* 2005, **251**, 429–433.
31 P. A. Kurian, C. Vijayan, K. Sathiyamoorthy, C. S. SuchandSandeep and R. Philip, *Nanoscale Res. Lett*. 2007, **2**, 561–568.
32 M. Hari, S. Mathew, B. Nithyaja, S. A. Joseph, V. P. N. Nampoori and P. Radhakrishnan, *Opt. Quant. Electron* 2012, **43**, 49–58.
33 H. Jiang, *J. Phys. Chem. C* 2012, **116**, 7664–7671.
34 F. Wun, A. H. Liu, H. Zheng, H. T. Chang, P. Shi, K. X. Cheng and X. M. Cheng, *Phys. E* 2012, **44**, 1158–1161.
35 K. P. Wang, J. Wang, J. T. Fan, M. Lotya, A. ÓNeill D. Fox, Y. Y. Feng, X. Y. Zhang, B. X. Jiang, Q. Z. Zhao, H. Z. Zhang, J. N. Coleman, L. Zhang and W. J. Blau. *ACS Nano* 2013, **7**, 9260–9267.
36 Q. Y. Ouyang, H. L. Yu, Z. Xu, Y. Zhang, C. Y. Li, L. H. Qi andY. J. Chen, *Appl. Phys. Lett.* 2013, **102**, 031912.
37 F. Li and X. G. Li, *Opt. Commun.* 2012, **285**, 5217–5222.
38 M. Fakis, G. Tsigardas, I. Polyzos, V. Giannetas, P. Persephonis, I. Spiliopoulos and J. Mikroyannidis, *Chem. Phys. Lett.* 2001, **342**, 155–161.
39 Q. Y. Ouyang, Y. J. Chen and C. Y. Li, *Mater. Chem. Phys.* 2012, **134**, 80–86.